DANISH METEOROLOGICAL INSTITUTE

—— SCIENTIFIC REPORT ——

98-14

The Back-Propagation Method for Inversion of Radio Occultation Data

By

Mette Dahl Mortensen

DMI

COPENHAGEN 1998

The Back-Propagation method for Inversion of Radio Occultation Data

Mette Dahl Mortensen

Danish Meteorological Institute
Denmark

July, 1998

Contents

1 Introduction

The radio occultation measurements are performed by a low Earth orbiting satellite (LEO) which measures the signals from a GPS satellite while the LEO sets behind the limb of the Earth relative to the GPS satellite.

When inverting radio occultation measurements of the atmosphere of the Earth a geometrical optics approach is usually taken. In this approximation the wave propagation is approximated by rays. The geometrical optics approximation is valid in the limit $\lambda \rightarrow 0$ where λ denotes the wavelength. This is usually a good approximation but due to the vertical gradient in the refractive index in the atmosphere the vertical resolution obtained by using the geometrical optics approximation will be diffraction limited. In cases where the vertical gradient in the refractivity is very large multipath problems will furthermore occur. Multipath problems is when several rays arrive at the receiver a the same time making it impossible to distinguish the ray path for the separate rays. In this case the geometrical optics approximation is invalid and better retrieval methods must be used.

This report is about an inversion method termed Back-propagated Abel inversion which can be used for overcoming diffraction problems when inverting radio occultation data for the atmosphere of the Earth. The method has previously been described in [Gorbunov and Gurvich, 1998] and [Karayel and Hinson, 1997]. The purpose of this report is to give a description of the method - containing details about the calculations which are omitted in [Gorbunov and Gurvich, 1998] and [Karayel and Hinson, 1997]. Furthermore, a few example of the results are given.

In the Back-propagated Abel inversion method the electromagnetic field is back-propagated using the solution to the wave equation in free space. When the field is back propagated to a plane much closer to the atmosphere the geometrical optics approach can be used in this plane but giving an enhanced resolution and less multipath problems. The idea is equivalent to a lens focusing problem.

Sharp gradients in the refractivity of the atmosphere can for example occur around the tropopause, where the temperature changes a lot. But otherwise sharp refractivity gradients will be seen close to the surface of the Earth most offend and will be caused by inversion layers and water vapor gradients.
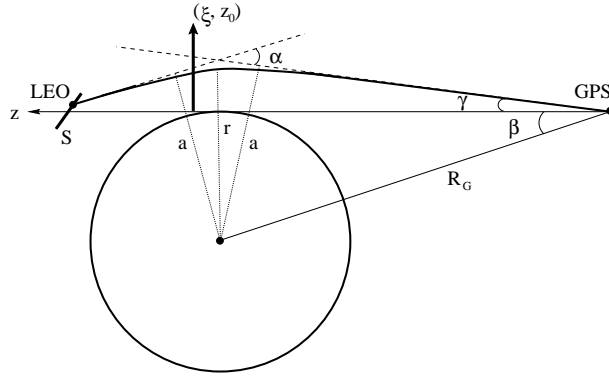
Figure 1: The geometry of the occultation and the coordinate system used for the back-propagation.

2   The Back-Propagated Abel inversion method

2.1   The Geometry

A schematic illustration of the occultation geometry is shown in Figure 1.

The distance to the GPS satellite is given by R_g. For each sample in the occultation measurement a coordinate system (z, ξ) is defined in the plane given by the position of the GPS and the LEO satellites and the center of the Earth. The $z-$axis is the vector from the GPS satellite tangential to the Earth closest to the LEO satellite. The $\xi-$axis is perpendicular to the Earth at the tangent point. The angle β is the angle between the vector $\vec{R}_g$ and $\hat{z}$. During the occultation the LEO satellite will move along S.

Figure 1 also illustrates a ray path. When using a geometrical optics approximation the signal from the GPS to the LEO satellite will follow a distinct ray path. The angle between the ray path and the $\hat{z}$-axis is denoted by γ. The closest distance to the Earth is given by r and the right-angled distance to the straight line asymptote of the ray path is a. The angle between the two asymptotes is α.

2.2   Determining the Coordinate System

For each sample in the occultation measurement a coordinate system (ξ, z) is defined. The coordinate system lies in the plane given by the GPS and the LEO positions and the center of the Earth. The $\hat{z}$-axis is defined by the straight line from the GPS towards the LEO tangent to the Earth. $z = 0$ at the tangent point. The $\hat{\xi}$-axis is perpendicular to the Earth and directed outwards.

The occultation measurements gives positions in a Cartesian coordinate system (x, y, z) with center at the center of the Earth. These coordinates must then be transformed to the new coordinates (ξ, z).

The equation for the plane going through the GPS-position, the LEO position and the center of the Earth is given by

$$(y_G z_L - z_G y_L)x + (z_G x_L - x_G z_L)y + (x_G y_L - x_L y_G)z = 0 \tag{1}$$

The coordinate system (ξ, z) will be in this plane so first a transformation from (x, y, z) to a coordinate system (x_1, y_1, z_1) with axes $\hat{x}_1$ and $\hat{z}_1$ in the GPS, LEO, Earth-center-plane. This transformation can be obtained by two rotations described by the angles φ and θ. Thus, the transformation from (x_1, y_1, z_1) to (x, y, z) is given as

$$\begin{bmatrix} x \\ y \\ z \end{bmatrix} = \begin{bmatrix} \cos\varphi & -\sin\varphi\cos\theta & -\sin\varphi\sin\theta \\ \sin\varphi & \cos\varphi\cos\theta & \cos\varphi\sin\theta \\ 0 & -\sin\theta & \cos\theta \end{bmatrix} \begin{bmatrix} x_1 \\ y_1 \\ z_1 \end{bmatrix} \tag{2}$$

and the transformation from (x, y, z) to (x_1, y_1, z_1) is given by

$$\begin{bmatrix} x_1 \\ y_1 \\ z_1 \end{bmatrix} = \begin{bmatrix} \cos\varphi & \sin\varphi & 0 \\ -\sin\varphi\cos\theta & \cos\varphi\cos\theta & -\sin\theta \\ -\sin\varphi\sin\theta & \cos\varphi\sin\theta & \cos\theta \end{bmatrix} \begin{bmatrix} x \\ y \\ z \end{bmatrix} \tag{3}$$

The angles φ and θ can be found from the equation for the GPS, LEO, Earth-center-plane

$$\tan\varphi = \frac{z_G y_L - y_G z_L}{z_G x_L - x_G z_L} \tag{4}$$

and

$$\tan\theta = \frac{x_L y_G - x_G y_L}{(z_G x_L - x_G z_L)\cos\varphi - (y_G z_L - z_G y_L)\sin\varphi} \tag{5}$$

The equation describing the Earth's ellipsoid is given by

$$x^2 + y^2 + \frac{z^2}{(1-f)^2} = R_{eq}^2 \tag{6}$$

where R_{eq} is the radius of the Earth at the equator and f is the oblateness. The ellipse determined by this equation in the GPS,LEO,Earth-center-plane will have $y_1 = 0$ and thus be given by

$$x_1^2 + z_1^2 \left(\sin^2\theta + \frac{1}{(1-f)^2}\cos^2\theta \right) = R_{eq}^2 \tag{7}$$

So when using

$$a_0 = R_{eq} \tag{8}$$

and

$$b_0 = \frac{R_{eq}}{\sqrt{\sin^2 \theta + \frac{1}{(1-f)^2} \cos^2 \theta}} \tag{9}$$

the ellipse can be written

$$\frac{x_1^2}{a_0^2} + \frac{z_1^2}{b_0^2} = 1. \tag{10}$$

Now the line from the GPS tangent to the ellipse can be determined. First, a parametric representation of the line is written

$$\begin{bmatrix} x_1 \\ z_1 \end{bmatrix} = \begin{bmatrix} x_{1,t} + t \\ \pm b_0 \sqrt{1 - \frac{x_{1,t}^2}{a_0^2}} \mp t \frac{b_0 x_{1,t}}{a_0 \sqrt{a_0^2 - x_{1,t}^2}} \end{bmatrix} \tag{11}$$

where $x_{1,t}$ is the x_1-coordinate of the tangent point on the ellipse and t is the parameter of the line. This line must go through the point $(x_{1,GPS}, z_{1,GPS})$. From this knowledge the point $x_{1,t}$ can be determined

$$x_{1,t} = \frac{-2b_0^2 x_{1,GPS} \pm \sqrt{4b_0^4 x_{1,GPS}^2 + 4(z_{1,GPS}^2 + \frac{b_0^2}{a_0^2} x_{1,GPS}^2)(z_{1,GPS}^2 - b_0^2)a_0^2}}{-2(z_{1,GPS}^2 + \frac{b_0^2}{a_0^2} x_{1,GPS}^2)} \tag{12}$$

The corresponding z_1-coordinate will be given by the equation for the ellipse

$$z_{1,t} = \pm b_0 \sqrt{1 - \frac{x_{1,t}^2}{a_0^2}} \tag{13}$$

Of the four solutions that can be obtained this way only two are real solutions. The correct sign for $z_{1,t}$ can be determined by testing the original equation for the tangent line (11). Thus, the two possible tangent lines are determined. Of these two the one closest to the LEO are the desired solution.

From the tangent line the new $\hat{z}$-axis can be determined as

$$\hat{z} = \frac{1}{\sqrt{(x_{1,t} - x_{1,GPS})^2 + (z_{1,t} - z_{1,GPS})^2}} \begin{bmatrix} x_{1,t} - x_{1,GPS} \\ z_{1,t} - z_{1,GPS} \end{bmatrix} \tag{14}$$

The rotation angle of $\hat{z}$ with respect to the $\hat{x}_1$-axis is given by

$$\cos v = \pm \hat{x}_1 \cdot \hat{z} \tag{15}$$

where the positive sign must be used when $z_{1,t} > z_{1,GPS}$ and the negative sign when $z_{1,t} < z_{1,GPS}$.

The transformation from (x_1, z_1)-coordinates to (ξ, z)-coordinates will thus be

$$\begin{bmatrix} \xi \\ z \end{bmatrix} = \begin{bmatrix} (x_1 - x_{1,t}) \sin v - (z_1 - z_{1,t}) \cos v \\ (x_1 - x_{1,t}) \cos v + (z_1 - z_{1,t}) \sin v \end{bmatrix} \tag{16}$$

As the GPS and the LEO satellite moves during the occultation the samples will not lie in the same plane during the occultation. The new coordinate system (ξ, z) is thus slowly rotating and translating with respect to the coordinate system (x, y, z).

2.3 Inversion using Back-Propagation

The method which has been used in the study presented here has previously been described in [Gorbunov et al., 1996] and [Gorbunov and Gurvich, 1998]. The idea is to use scalar diffraction theory to back-propagate the complex electro-magnetic field measured at the LEO to a plane nearer to the Earth. Once this is done the geometrical optics approximation can be applied again but the diffraction effects will be smaller.

To obtain the back-propagation solution the propagation of the electro-magnetic signal must be described. The complex amplitude u of the scalar electro-magnetic field in vacuum satisfies the Helmholtz equation

$$\Delta u + k^2 u = 0 \tag{17}$$

where k is the free space wave number. The scalar version of the wave equation can be used because the atmosphere is tenuous [Tartarskii, 1971].

If the electro-magnetic field u_0 is known all over a distant straight line S a solution $u(\vec{x})$ to the Helmholtz equation can be found in a given point $\vec{x}$. This is the two dimensional solution for the external boundary problem for the Helmholtz equation [Born and Wolf, 1993]

$$u(x) = \frac{i}{2} \int\limits_{S} u_0(y) \frac{\partial}{\partial n_y} H_0^{(1)}(k|\vec{x} - \vec{y}|) \, dS_y \tag{18}$$

where n_y is the external normal to S and $H_0^{(1)}$ is the Hankel function of first kind of zero order.

The two dimensional approximation can be used under the assumption that the horizontal structures in the atmosphere are large compared to the lateral dimensions of the Fresnel zone. The Fresnel zone is a measure of the area which has influence on the measurement.

In an occultation measurement of the Earth the Fresnel zone size is less than 2km so the two dimensional approximation is normally good.

The high frequency expansion $(k|\vec{x} - \vec{y}|) \to \infty$ of $H_0^{(1)}$ in the expression for the field (18) is given by

$$H_0^{(1)}(k|\vec{x} - \vec{y}|) \simeq \sqrt{\frac{2}{\pi k|\vec{x} - \vec{y}|}} \exp\left(ik|\vec{x} - \vec{y}| - i\frac{\pi}{4}\right) \tag{19}$$

when using this the expression for the field becomes

$$u(\vec{x}) = \left(\frac{k}{2\pi}\right)^{1/2} \int_S u_0(\vec{y}) \cos \varphi_{xy} \frac{\exp(ik|\vec{x} - \vec{y}| - i\pi/4)}{|\vec{x} - \vec{y}|^{1/2}} \, dS_y \tag{20}$$

where φ_{xy} is the angle between the normal $\vec{n_y}$ to S and the vector $\vec{x} - \vec{y}$. This solution can be used to described the field measured at the LEO if the field is known on the back-propagation line (ξ, z_0) indicated in Figure 1.

In order to describe the field at the back-propagation line from the field measured at the LEO the solution to boundary problem which propagates in the opposite direction must be chosen. This solution is given by

$$u(\vec{x}) = \left(\frac{k}{2\pi}\right)^{1/2} \int_S u_0(\vec{y}) \cos \varphi_{xy} \frac{\exp(-ik|\vec{x} - \vec{y}| + i\pi/4)}{|\vec{x} - \vec{y}|^{1/2}} \, dS_y \tag{21}$$

In this case S is the curve formed by the movement of the LEO satellite during the occultation and $u_0(\vec{y})$ is the measured signal. Due to the large radius of the satellite orbit and the short duration of the occultation measurement S can be approximated by a straight line. The vector $\vec{x}$ now indicates a point on the back-propagation line. The field $u(\vec{x})$ is thus the complex electro-magnetic back-propagated signal which can be used to derive the geometrical optics solution.

Using the (ξ, z)-coordinate system the $\vec{x}$-vector is given by (ξ, z_0) and the measurement vector $\vec{y}$ can be described by the parametric equation

$$\vec{r}(\xi) = \begin{bmatrix} 1 \\ a \end{bmatrix} \xi + \begin{bmatrix} 0 \\ b \end{bmatrix} \tag{22}$$

where a and b are known constants as the position of the LEO satellite is known. The normal vector $\vec{n_y}$ will then be given by

$$\vec{n}_y = \begin{bmatrix} -1 \\ \frac{1}{a} \end{bmatrix} \tag{23}$$

so the angle φ_{xy} can be found from

$$\cos\varphi_{xy} = \frac{\vec{n}_y \cdot (\vec{x}-\vec{y})}{|\vec{n}_y||\vec{x}-\vec{y}|} \tag{24}$$

Finally, the integration can be transformed from the curve S to the variable ξ whereby the back-propagation integral becomes

$$u(\vec{x}) = \left(\frac{k}{2\pi}\right)^{1/2} \int_{-\infty}^{\infty} u_0(\vec{y})\cos\varphi_{xy}\frac{\exp(ik|\vec{x}-\vec{y}|-i\pi/4)}{|\vec{x}-\vec{y}|^{1/2}}\sqrt{1+a^2}\,d\xi \tag{25}$$

The back-propagation solution assumes stationarity in time as the occultation samples used to calculate the back-propagated field are in reality a time series. This is a good approximation for the atmosphere as the occultation measurement only takes about a minute during which time interval the atmosphere can not change significantly. On the other hand the back-propagation solution also assumes that the GPS does not move during the occultation as the measurements are assumed to originate from the same place in the back-propagation solution. This is not entirely true but since the distance to the GPS satellite is very large compared to the distance from the atmosphere to the LEO the GPS satellite can be assumed to be at a fixed location during the occultation.

2.4   Geometrical Optics Inversion

The inversion of radio occultation data using the geometrical optics approximation is the most commonly used inversion method for this type of data. The method has been extensively described elsewhere e.g. [Fjeldbo et al., 1971], [Melbourne et al., 1994], [Kursinski et al., 1997]. Thus, in here only a brief review of the method will be given.

In the geometrical optics approximation, the electro-magnetic signal is described as following distinct ray paths. A ray passing through the atmosphere is refracted according to Snell's law due to the variation of the refractive index. The total influence of the atmosphere on the signal can be described by a bending angle α, an impact parameter a and a tangent radius r. These parameters are shown in Figure 1. As the Earth is ellipsoidal (not shown in Figure 1) the local center of the refraction and the local radius of curvature should be used in this calculation instead of the center of the Earth and the Earth radius [Syndergaard, 1998].

The geometrical optics solution can either be used directly on the measured signal or it can be applied after the back-propagation.

When the geometrical optics approach is used directly a, α can be calculated from the measured Doppler-shifted frequency of the transmitter signal at the receiver and the

positions and velocities of the satellites for each sample in the occultation measurement [Fjeldbo et al., 1971].

In the case where the field has been back propagated the approach is different as the time dependence is lost as the samples are combined to form the back-propagated field. To find the bending angle and the impact parameter the total phase delay ϕ as a function of height ξ on the back-propagation line must be calculated from the complex back-propagated signal. Then the bending angle α is given by

$$\alpha - \gamma = \arcsin\left(\frac{-\lambda}{2\pi}\frac{d\phi}{d\xi}\right) \tag{26}$$

and the impact parameter a is given by

$$a_{2D} = (z_0 - z_R)\sin(\alpha - \gamma) + (\xi - \xi_R)\cos(\alpha - \gamma) \tag{27}$$

$$a = \sqrt{a_{2D}^2 + y_{1,R}^2} \tag{28}$$

where the angle γ can be determined from $\gamma = \arcsin(\frac{a}{R_G}) - \beta$ and $\beta = \arcsin(\frac{R_e}{R_G})$. The distance from the GPS satellite to the center of the Earth is denoted by R_G and R_e is the Earth radius [Karayel and Hinson, 1997]. The center of refraction is given by $(\xi_R, z_R, y_{1,R})$ where $y_{1,R}$ is the contribution that lies outside the (ξ, z)-plane.

If the refractive index varies only with radius the conversion from bending angles α as a function of impact height a to refractivity n is performed through the Abel transform [Fjeldbo et al., 1971]

$$n(r) = \exp\left[\frac{1}{\pi}\int_{a_1}^{\infty}\frac{\alpha(a)}{\sqrt{a^2 - a_1^2}}\,da\right] \tag{29}$$

where $a_1 = nr$ is the impact parameter for the ray whose tangent radius is r.

The refractive index primarily depends on the dry neutral atmosphere, free electrons in the ionosphere and water vapor [Kursinski et al., 1997]. The ionospheric influence is frequency dependent and can thus be removed as the GPS transmit two different frequencies. In general the dry neutral atmosphere and the water vapor can not be separated. In this study the main interest has been in studying the inversion process to refractivity. Therefore refractivity has been converted to dry temperature results assuming no water vapor. This is only a matter of a convenient way of representing the results. The results are not limited to this case.

2.5   Discussion

The back-propagation solution (21) is the solution for free space propagation. In order to enhance the resolution the back-propagation line will be placed far into the atmosphere of the Earth. The field obtained is thus not equal to the physical field that would be measured at this point. This is not a problem though as the bending angle and impact parameter still can be calculated using the geometrical optics approximation as shown in Figure 1. Only, the parameters will be filtered so they have an enhanced resolution. The exact position of the back-propagation line is a free parameter.

When using the back-propagation solution horizontal homogeneity is assumed in the entire area covered by the occultation. This area includes the horizontal area perpendicular to the signal propagation direction which is created by the satellite movement in this direction. In the direction of the signal propagation the horizontal resolution and thereby the area where homogeneity must be assumed is estimated to be equal to the ray path propagation length inside one vertical resolution cell. Both these assumptions also applies to the direct solution using the geometrical optics approach. As the back-propagation solution gives a very good vertical resolution the measure for the horizontal resolution in the direction of the signal propagation will also be improved. Thus, when considering the area in which the horizontal structure should be homogeneous the movement of the center of refractivity should be taken into account.

In the back-propagation integral (21) the integration limits are infinite. To evaluate this integral as fast as possible the stationary phase point was found, i.e., the extremum point of the function $\varphi = arg(u_0(y)) - k|\vec{x} - \vec{y}|$. It was then found that using integration limits equivalent to phase variations $\varphi \pm 10\pi$ made the integral converge [Gorbunov et al., 1996]. Choosing a narrow integration interval will also have the effect of decreasing the influence from noise on the back-propagated results [Marouf et al., 1986]. In cases where very high resolution is needed in order to retrieve a structure wider integration limits will be necessary [Marouf et al., 1986].

As the back-propagation solution is a rather slow method compared to using the geometrical optics approximation directly at the measured data the two methods are normally combined. Multipath propagation in the neutral atmosphere is normally only seen for low altitudes so the back-propagation method is used in the lower part of the measurement while the direct geometrical optics approximation is used in the upper part. The two solutions can easily be combined as both calculate bending angles as a function of impact parameter and in areas where the atmosphere is smooth the two solutions will be equal.

3 Examples

In this section the results obtainable with the back-propagation method will be illustrated. This done by comparing inversions of simulated occultation data using the back-propagation method and using the geometrical optics approach directly at the measurements. A more thorough comparison can be found in [Mortensen et al., 1998].

In the following the inversions obtained using the back-propagation method will be termed back-propagated Abel inversion. The inversion obtained using the geometrical optics approach directly at the measurement will be termed direct Abel inversion.

The back-propagation plane is set at $z = 100km$. This placement is suitable for most inversion cases but is not an optimized position in any way.

For a smooth atmosphere the Back-propagated Abel inversion and the Direct Abel inversion should give the same results. A simulation of an occultation measurement has been performed using three dimensional ray tracing through a smooth model atmosphere [Høeg et al., 1995] with no water vapor. The simulation used orbit epherimedes from the GPS/MET experiment occultation no. 1 Oct. 14, 1995. The neutral atmosphere has been modeled using the MSIS model and the ionosphere has been modeled using a simple two-layer exponential model (Chapman layers). In the simulation an ellipsoidal Earth was used. Figure 2 shows the model refractivity used as input for the simulation together with the refractivity retrieved using the back-propagated Abel inversion. As can be seen from the figure there is very good agreement between the model profile and the retrieved profile.

Figure 3 shows the error in retrieved refractivity relative to the model refractivity. In this figure results are shown for both the back-propagated Abel inversion (BA) and the direct Abel inversion (DA). As expected the error profile for both methods are similar. From 35km and downwards the error for both methods are less than 0.1%. Above 35km the error increases due to limitations in the ionosphere correction method.

In cases where the atmosphere contains large gradients there will be substantial difference between the back-propagated Abel inversion result and the direct Abel inversion result. A one dimensional forward occultation simulator which takes into account diffraction has been developed at JPL, i.e., large gradients can be simulated. The model uses a spherical Earth, spherical satellites orbit and a piecewise linear temperature profile as atmosphere model [Kursinski et al., 1997]. Forward simulation data from this model has been provided by Roger E. Linfield and Rob Kursinski, JPL.

Figure 4 shows part of the refractivity profile for a simulation with a large gradient. Both the model data and the back-propagated Abel inversion result is shown. The figure again shows very good agreement between the model data and the retrieved result.
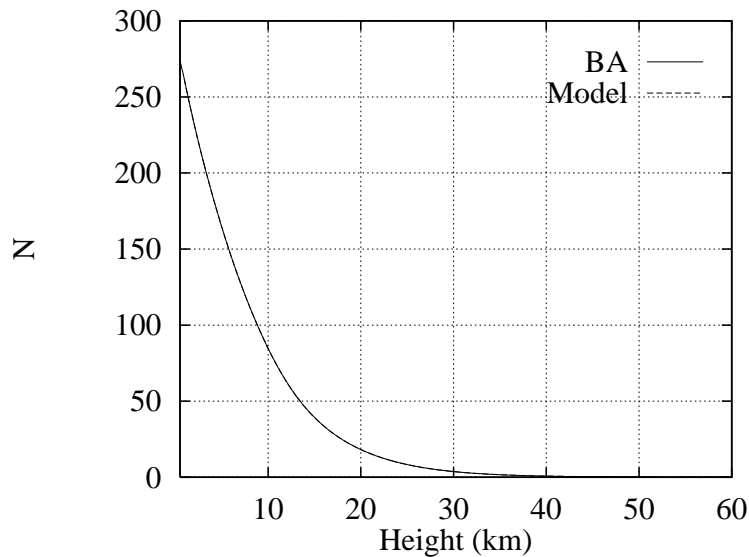
Figure 2: Model refractivity and result obtained after inversion of the simulated occultation data using the back-propagated Abel inversion. Smooth atmosphere case.
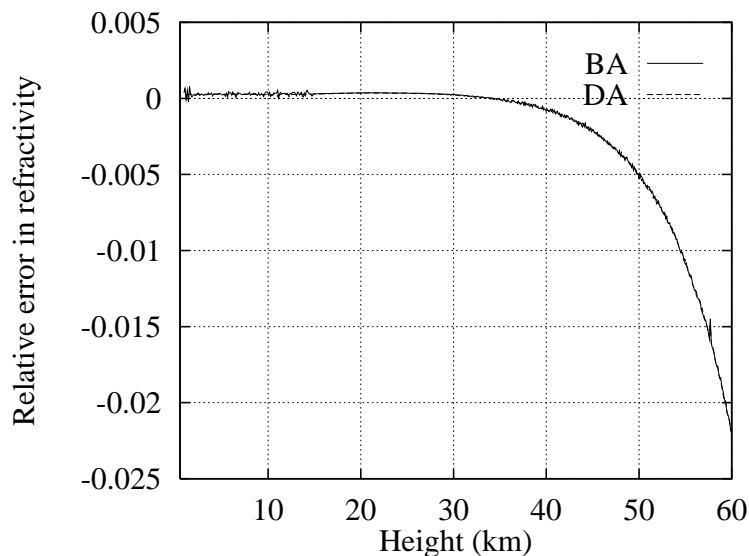

Figure 3: Error in derived refractivity for the back-propagated Abel inversion (BA) and the direct Abel inversion (DA). Seen relative to the model refractivity. Smooth atmosphere case.

In Figure 5 the error relative to the model result is shown for both the back-propagated Abel inversion and for the direct Abel inversion. The back-propagated Abel inversion gives errors less than 0.1% as in the previous case whereas the error for the direct Abel inversion is more than 1% in some places and generally worse than seen in the smooth case. The direct Abel inversion gives rather bad results in a large area around the large
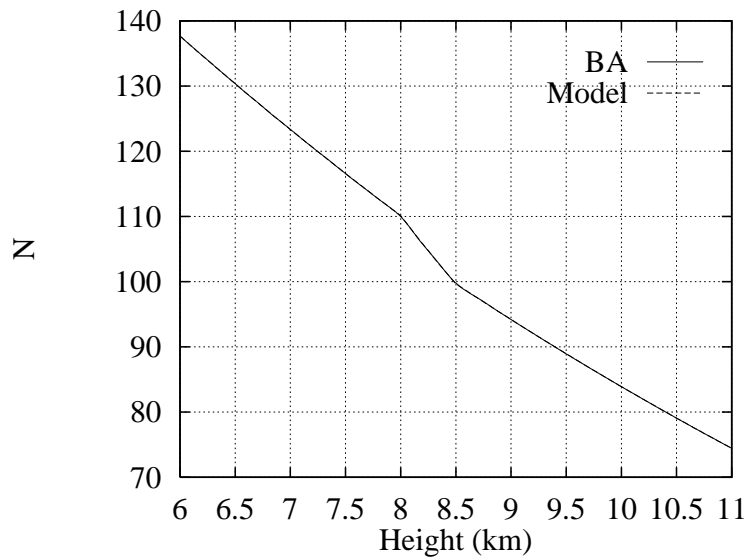
Figure 4: Window of model refractivity and result obtained after inversion of the simulated occultation data using the back-propagated Abel inversion. For Atmosphere with large gradient.
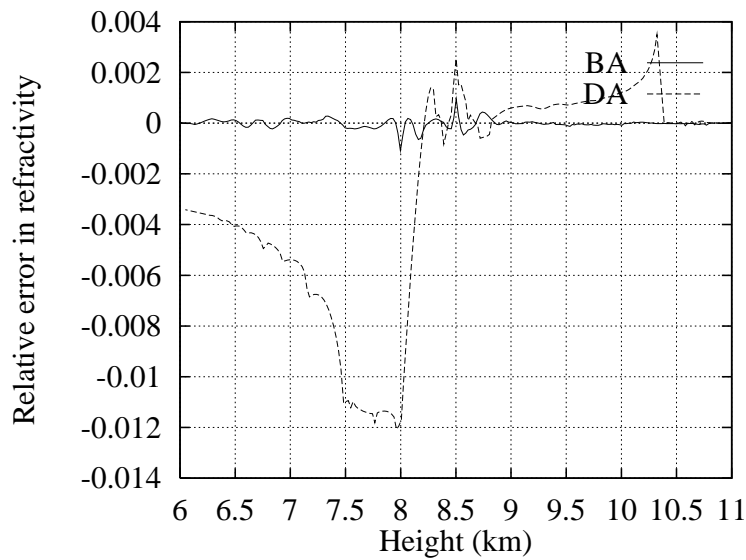

Figure 5: Window of error in derived refractivity for the back-propagated Abel inversion (BA) and the direct Abel inversion (DA). Seen relative to the model refractivity. For Atmosphere with large gradient.

gradient. This is because the direct Abel inversion can not take diffraction effects into account and these are seen several kilometers before and after the actual occurrence of the large gradient in this case. Furthermore, the gradient shown in Figure 4 is so large that multipath occurs. When multipath is present the direct Abel inversion is strictly not

valid as a single ray cannot be identified. This is the reason for the very large errors in some areas.

4 Conclusions

In this report the Back-propagated Abel inversion for inversion of radio occultation measurements has been described. This method has very good vertical resolution and can overcome most multipath problems. The accuracy in smooth areas are as good as the direct Abel inversion and large gradient are resolved with high accuracy also. The method is as the direct Abel inversion based on an assumption of spherical symmetry.

The computational effort involved in using the Back-propagated Abel inversion is substantially larger than the effort involved in calculating the direct Abel inversion. On the other hand the results obtained using the Back-propagated Abel inversion is superior to the results obtained with the direct Abel inversion in areas with large gradients and as good as the direct Abel inversion in smooth areas. In general it must thus be recommended to use the Back-propagated Abel inversion for inversion of radio occultation data.

References

[Born and Wolf, 1993] Born, M. and Wolf, E. (1993). *Principles of Optics*. Pergamon Press, Oxford, England, 6 edition.

[Fjeldbo et al., 1971] Fjeldbo, G., Kliore, J., and Eshleman, V. (1971). The neutral atmosphere of Venus as studied with the Mariner V radio occultation experiments. *The Astronomical Journal*, 76:123–140.

[Gorbunov et al., 1996] Gorbunov, M., Gurvich, A., and Bengtsson, L. (1996). Advanced algorithms of inversion of GPS/MET satellite data and their application to reconstruction of temperature and humidity. Technical report, Max-Planck-Institute for Meteorology, Hamburg.

[Gorbunov and Gurvich, 1998] Gorbunov, M. and Gurvich, A. S. (1998). Microlab-1 experiment: Multipath effects in the lower troposphere. *Journal of Geophysical Research*, 103(D12):13,819–13,826.

[Høeg et al., 1995] Høeg, P., Hauchecorne, A., Kirhcengast, G., Syndergaard, S., Belloul, B., Leitinger, R., and Rothleitner, W. (1995). Derivation of atmospheric properties using radio occultation technique. Scientific Report 95-4, Danish Meteorological Institute.

[Karayel and Hinson, 1997] Karayel, E. T. and Hinson, D. P. (1997). Sub-fresnel-scale vertical resolution in atmospheric profiles from radio occultation. *Radio Science*, 32:411–423.

[Kursinski et al., 1997] Kursinski, E., Hajj, G., Hardy, K., Schofield, J., and Linfield, R. (1997). Observing earth's atmosphere with radio occultation measurementes using GPS. *J. Geophys. Res.*, 102(D19):23,429–23,465.

[Marouf et al., 1986] Marouf, E. A., Tyler, G., and Rosen, P. (1986). Profiling Saturn's rings by radio occultation. *ICARUS*, 68:120–166.

[Melbourne et al., 1994] Melbourne, W., Davis, E., Duncan, C., Hajj, G., Hardy, K., Kursinski, E., Meehan, T., Young, L., and Yunck, T. (1994). The application of spaceborne GPS to atmospheric limb sounding and global change monitoring. JPL Publication 94-18, JPL, Pasadena, CA, USA.

[Mortensen et al., 1998] Mortensen, M., Linfield, R., and Kursinski, E. (1998). Vertical resolution approaching 100m for GPS occultations of the Earth's atmosphere. *Submitted to Radio Science*.

[Syndergaard, 1998] Syndergaard, S. (1998). Modeling the impact of the earth's oblateness on the retrieval of temperature and pressure profiles from limb sounding. *Journal of Atmospheric and Solar-Terrestrial Physics*, Vol. 60(No. 2):pp. 171–180.

[Tartarskii, 1971] Tartarskii, W. I. (1971). *The effects of the Turbulent Atmosphere on Wave Propagation.* Natl. Tech. Inf. Serv., Springfield, Va.

DANISH METEOROLOGICAL INSTITUTE

Scientific Reports

Scientific reports from the Danish Meteorological Institute cover a variety of geophysical fields, i.e. meteorology (including climatology), oceanography, subjects on air and sea pollution, geomagnetism, solar-terrestrial physics, and physics of the middle and upper atmosphere.

Reports in the series within the last five years:

No. 94-1
Bjørn M. Knudsen: Dynamical processes in the ozone layer.

No. 94-2
J. K. Olesen and K. E. Jacobsen: On the atmospheric jet stream with clear air turbulences (CAT) and the possible relationship to other phenomena including HF radar echoes, electric fields and radio noise.

No. 94-3
Ole Bøssing Christensen and Bent Hansen Sass: A description of the DMI evaporation forecast project.

No. 94-4
I.S. Mikkelsen, B. Knudsen, E. Kyrö and M. Rummukainen: Tropospheric ozone over Finland and Greenland, 1988-94.

No. 94-5
Jens Hesselbjerg Christensen, Eigil Kaas, Leif Laursen: The contribution of the Danish Meteorological Institute (DMI) to the EPOCH project "The climate of the 21st century" No. EPOC-003-C (MB).

No. 95-1
Peter Stauning and T.J. Rosenberg: High-Latitude, Day-time Absorption Spike Events
1. Morphology and Occurrence Statistics.
Not Published.

No. 95-2
Niels Larsen: Modelling of changes in stratospheric ozone and other trace gases due to the emission changes : CEC Environment Program Contract No. EV5V-CT92-0079. Contribution to the final report.

No. 95-3
Niels Larsen, Bjørn Knudsen, Paul Eriksen, Ib Steen Mikkelsen, Signe Bech Andersen and Torben Stockflet Jørgensen: Investigations of ozone, aerosols, and clouds in the arctic stratosphere : CEC Environment Program Contract No. EV5V-CT92-0074. Contribution to the final report.

No. 95-4
Per Høeg and Stig Syndergaard: Study of the derivation of atmospheric properties using radio-occultation technique.

No. 95-5
Xiao-Ding Yu, **Xiang-Yu Huang** and **Leif Laursen** and Erik Rasmussen: Application of the HIRLAM system in China: Heavy rain forecast experiments in Yangtze River Region.

No. 95-6
Bent Hansen Sass: A numerical forecasting system for the prediction of slippery roads.

No. 95-7
Per Høeg: Proceeding of URSI International Conference, Working Group AFG1 Copenhagen, June 1995. Atmospheric Research and Applications Using Observations Based on the GPS/GLONASS System.

No. 95-8
Julie D. Pietrzak: A Comparison of Advection Schemes for Ocean Modelling.

No. 96-1
Poul Frich (co-ordinator), H. Alexandersson, J. Ashcroft, B. Dahlström, G.R. Demarée, A. Drebs, A.F.V. van Engelen, E.J. Førland, I. Hanssen-Bauer, R. Heino, T. Jónsson, K. Jonasson, L. Keegan, P.Ø. Nordli, **T. Schmith**, **P. Steffensen**, H. Tuomenvirta, O.E. Tveito: North Atlantic Climatological Dataset (NACD Version 1) - Final Report.

No. 96-2
Georg Kjærgaard Andreasen: Daily Response of High-latitude Current Systems to Solar Wind Variations: Application of Robust Multiple Regression. Methods on Godhavn magnetometer Data.

No. 96-3

Jacob Woge Nielsen, Karsten Bolding Kristensen, Lonny Hansen: Extreme sea level highs: A statistical tide gauge data study.

No. 96-4
Jens Hesselbjerg Christensen, Ole Bøssing Christensen, Philippe Lopez, Erik van Meijgaard, Michael Botzet: The HIRLAM4 Regional Atmospheric Climate Model.

No. 96-5
Xiang-Yu Huang: Horizontal Diffusion and Filtering in a Mesoscale Numerical Weather Prediction Model.

No. 96-6
Henrik Svensmark and Eigil Friis-Christensen: Variation of Cosmic Ray Flux and Global Cloud Coverage - A Missing Link in Solar-Climate Relationships.

No. 96-7
Jens Havskov Sørensen and Christian Ødum Jensen: A Computer System for the Management of Epidemiological Data and Prediction of Risk and Economic Consequences During Outbreaks of Foot-and-Mouth Disease. CEC AIR Programme. Contract No. AIR3 - CT92-0652.

No. 96-8
Jens Havskov Sørensen: Quasi-Automatic of Input for LINCOM and RIMPUFF, and Output Conversion. CEC AIR Programme. Contract No. AIR3 - CT92-0652.

No. 96-9
Rashpal S. Gill and Hans H. Valeur: Evaluation of the radarsat imagery for the operational mapping of sea ice around Greenland.

No. 96-10
Jens Hesselbjerg Christensen, Bennert Machenhauer, Richard G. Jones, Christoph Schär, Paolo Michele Ruti, Manuel Castro and Guido Visconti: Validation of present-day regional climate simulations over Europe: LAM simulations with observed boundary conditions.

No. 96-11
Niels Larsen, Bjørn Knudsen, Paul Eriksen, Ib Steen Mikkelsen, Signe Bech Andersen and Torben Stockflet Jørgensen: European Stratospheric Monitoring Stations in the Artic: An European contribution to the Network for Detection of Stratospheric Change (NDSC): CEC Environment Programme Contract EV5V-CT93-0333: DMI contribution to the final report.

No. 96-12

Niels Larsen: Effects of heterogeneous chemistry on the composition of the stratosphere: CEC Environment Programme Contract EV5V-CT93-0349: DMI contribution to the final report.

No. 97-1
E. Friis Christensen og C. Skøtt: Contributions from the International Science Team. The Ørsted Mission - A Pre-Launch Compendium.

No. 97-2
Alix Rasmussen, Sissi Kiilsholm, Jens Havskov Sørensen, Ib Steen Mikkelsen: Analysis of Tropospheric Ozone Measurements in Greenland: Contract No. EV5V-CT93-0318 (DG 12 DTEE): DMI's contribution to CEC Final Report Arctic Trophospheric Ozone Chemistry ARCTOC.

No. 97-3
Peter Thejll: A Search for Effects of External Events on Terrestrial Atmospheric Pressure: Cosmic Rays

No. 97-4
Peter Thejll: A Search for Effects of External Events on Terrestrial Atmospheric Pressure: Sector Boundary Crossings

No. 97-5
Knud Lassen: Twentieth Century Retreat of Sea-Ice in the Greenland Sea

No. 98-1
Niels Woetman Nielsen, Bjarne Amstrup, Jess U. Jørgensen:
HIRLAM 2.5 parallel tests at DMI:
Sensitivity to type of schemes for turbulence, moist processes and advection

No. 98-2
Per Høeg, Georg Bergeton Larsen, Hans-Henrik Benzon, Stig Syndergaard, Mette Dahl Mortensen:
The GPSOS project
Algorithm Functional Design and Analysis of ionosphere, Stratosphere and Troposphere Observations

No. 98-3
Dahl Mortensen, Mette; Per Høeg:
Satellite Atmosphere Profiling Retrieval in a Nonlinear Troposphere
Previously entitled: Limitations Induced by Multipath

No. 98-4

Dahl Mortensen, Mette Per Høeg:
Resolution Properties in Atmospheric Profiling with GPS

No. 98-5
Gill, R. S. and M. K. Rosengren
Evaluation of the Radarsat Imagery for the Operational Mapping of Sea Ice around Greenland in 1997.

No. 98-6
Gill, R. S., Valeur, H. H., Nielsen, P. and Hansen, K. Q.: Using ERS SAR images in the operational mapping of sea ice in the Greenland waters: final report for ESA-ESRIN's: pilot projekt no. PP2.PP2.DK2 and 2nd Announcement of opportunity for the exploitation of ERS data projekt No. AO2..DK 102.

No. 98-7
Høeg, Per et al.: GPS Atmosphere Profiling Methods and Error Assessments.

No. 98-8
Svensmark, H., N. Woetmann Nielsen and A.M. Sempreviva: Large Scale Soft and Hard Turbulent States of the Atmosphere.

No. 98-9
Lopez, Philippe, Eigil Kaas and Annette Guldberg: The Full Particle-In-Cell advection scheme in spherical geometry**.**

No. 98-10
Svensmark, H.: Influence of Cosmic Rays on Earth's Climate.

No. 98-11
Thejll, Peter and Henrik Svensmark: Notes on the method of normalized multivariate regression.

No. 98-12
Lassen. K: Extent of sea ice in the Greenland Sea 1977-1997: an extension of DMI Scientific Report 97-5

No. 98-13
Larsen, Niels; Adriani, Alberto and Donfrancesco, Guido Di: Microphysical analysis oof plar stratospheric clouds observed by Lidar at McMurco, Antarctica

No.98-14
Dahl Mortensen, Mette: The Back-Propagation Method for Inversion of Radio Occultation Data.